frontiers | Frontiers in Earth Science

TYPE Original Research
PUBLISHED 12 January 2023
DOI 10.3389/feart.2022.1024710

OPEN ACCESS

EDITED BY
Chao Zhou,
China University of Geosciences
Wuhan, China

REVIEWED BY
Chaoying Zhao,
Chang'an University, China
Li Wang,
China Three Gorges University, China

*CORRESPONDENCE
Shaoqi Zhou,
comradeshaoqi@163.com

SPECIALTY SECTION
This article was submitted to
Geohazards and Georisks,
a section of the journal
Frontiers in Earth Science

RECEIVED 22 August 2022
ACCEPTED 31 October 2022
PUBLISHED 12 January 2023

CITATION
Shen C, Zhou S, Luo X, Zhang Y and
Liu H (2023), Using DInSAR to inventory
landslide geological disaster in Bijie,
Guizhou, China.
Front. Earth Sci. 10:1024710.
doi: 10.3389/feart.2022.1024710

Using DInSAR to inventory landslide geological disaster in Bijie, Guizhou, China

Chaoyong Shen[1,2,3], Shaoqi Zhou[2]*, Xuling Luo[3], Yu Zhang[2] and Hui Liu[4]

[1]Guizhou Academy of Sciences, Guiyang, China, [2]College of Resources and Environmental Engineering, Guizhou University, Guiyang, China, [3]The Third Surveying and Mapping Institute of Guizhou Province, Guiyang, China, [4]College of Resource Environment and Tourism, Capital Normal University, Beijing, China

Landslides are very complicated natural phenomena that create significant losses of life and assets throughout China. However, previous studies mainly focused on monitoring the development trend of known landslides in small areas, and few studies focused on the identification of new landslides. In addition, karst areas, where the vegetation is dense, the mountains are high, the slopes are steep, and the time incoherence is serious, have difficulty in tracking Differential Interferometric Synthetic Aperture Radar (DInSAR) landslides. Therefore, based on DInSAR technology, we use ALOS-2 PALSAR data to conduct continuous monitoring of existing hazards and identify new geological hazards in karst areas. The major results are as follows: 1) From June 11 to 6 August 2017, it was discovered that a hidden point of landslides occurred on the 420 m northwest mountain near the town of Zongling. It was determined that the landslide hidden point had been slipping for two consecutive years, with an average slip of 6.0 cm. From 4 September 2016 to 22 January 2017, undiscovered hidden points in the landslide account were found in Yinjiazhai. On 13 September 2016 and 22 November 2016, the discovered potential hazards in the landslide log book were the mountain hazards in southwestern Shiping village, and the deformation was 7.8 cm. 2) The DInSAR monitoring results from September to November 2016 showed that large deformations occurred in the landslide area of Shiping village. During a field visit, large cracks on the surface were found. The length of surface cracks in the southwest direction of Shiping village was 2.8 m. On 13 July 2017, Shiping collapsed as a result of the collapse of the mountainous area where the disaster occurred. The average slope of the landslide in the landslide area was approximately 65°, the height was 95 m, the length and width were 150 m and 25 m, respectively, and the thickness was 5 m. The method has shown great potential in precisely identifying some new geological hazards sites, as well as tracking and monitoring the potential hazards of geological disasters listed on the landslide account.

KEYWORDS

landslides, hidden point, exclusion investigation, DInSAR, deformation monitoring

1 Introduction

Landslide is a kind of global geological phenomenon that are triggered by external factors, including geological structure, stratum lithology, topography, meteorology, and human activities, due to a lack of vegetation in sloping areas or tectonic movement (Hu et al., 2016; Iverson, 2000; Malamud et al., 2004; Shen et al., 2019; Ji et al., 2020, Zhang et al., 2022). Depending on their intensity, landslides can be very devastating geological disasters similar to earthquakes and volcanic eruptions (Ali et al., 2020, Ali et al., 2021). From 2004 to 2016, landslide disasters caused nearly 60,000 human casualties worldwide (Froude and Petley, 2018). Furthermore, according to the National Plan for Geological Disaster Prevention and Control of China, the entire province of Guizhou is considered a geologically disaster-prone area. It is one of the hardest-hit areas in the country for geological disasters and has the characteristics of being "full, heavy, and numerous" (Zou et al., 2017). At present, a total of 11,161 geological disasters have been identified nationwide, of which 6,618 are hidden dangers to the human population, property, and infrastructure. Therefore, research on landslides and associated hazards is of great significance for sustainable development.

Over the past several decades, the monitoring of landslides and associated hazards has been carried out by patrolling disaster-prone areas on a daily basis. The daily patrol is often used in conjunction with levelling measurements, GPS measurements, 3D laser scanning, measuring robots, close-range photogrammetry, and other methods (Singhroy 2009; Yin et al., 2010; Alice et al., 2013). Most landslide hazards occur in densely vegetated steep mountainous areas. The complex terrain of landslide-prone areas coupled with the dense vegetation affects sightlines and long-distance observations, thus decreasing the effectiveness of the monitoring process. Moreover, the number of landslide hazards is high, and they are widely distributed. Therefore, a tremendous amount of laborious physical work is required for daily monitoring, which is very expensive and still insufficient. With the introduction of new technologies in the field of geology, the accuracy, efficiency, and reliability monitoring studies of geological hazards in complex terrain have been greatly improved. Therefore, many scholars have participated in researching landslide monitoring and analysis (Agostini et al., 2002; Ayalew et al., 2005; Wiatr et al., 2009; Zainon, 2011; Othman et al., 2012; Lei et al., 2013; Tai and Chang, 2015; Shen et al., 2019).

DInSAR is capable of taking high-spatial-resolution deformation data over a large area with higher accuracy and speed compared to the other traditional methods. Previously, DInSAR was applied to landslide surveys, landslide inventory, and modelling (Catani et al., 2005; Corsini et al., 2006). Tofani et al. (2013) integrated surface monitoring data and DInSAR data to monitor landslides in northern Italy, which led to a better understanding of the relationship between the regularity of landslide deformations and the driving forces of landslides. Moretti et al. (2013) introduced the pan-European Terrafirma landslide project. Komac et al. (2015) used DInSAR and GPS measurement methods to assess a landslide disaster in the field and compared its consistency with ground deformation over a period of time; they also assessed the consistency of the slope quality motion detection. Carla et al. (2016) determined several landslide areas that exceeded predetermined threshold and improved the accuracy by DInSAR technology; they also updated the rate of landslide areas through on-site verification for risk assessment and management rather than relying on experience and traditional methods.

The wavelength has a great influence on DInSAR results; thus, L-band ALOS-2 PALSAR data are widely used to inventory landslide disasters in densely vegetated areas. For example, Konishi and Suga (2018) used L-band ALOS-2 images to detect and map landslides triggered by the Kumamoto earthquake (7.0 Mw) in Kyoto covered by forest, grassland, and crops, which confirmed the potential of the technique in landslide detection and mapping. The same landslide event was studied by Aimaiti et al. (2019) using the same ALOS-2 images and the same performance metrics, proving that images taken along the descending track perform better than those taken along the ascending track because of the more favorable viewing angle.

Therefore, to effectively carry out investigations of landslide hazards in places like Guizhou karst geomorphological areas, we wanted to develop a method that could solve special terrain, climate, and vegetation condition constraints. For this purpose, we used long-range ALOS-2 PALSAR stripe model HH-polarization 3-m-resolution descending-track data and differential interferometry technology to carry out extensive monitoring of deformation in the disaster-prone area of Guizhou-Bijie, China. The method shows great potential by precisely identifying existing (and some new) geological hazard sites.

2 Materials and methods

2.1 Study area

The study area is located in Dafang County and Nayong County of Bijie City in the northwestern part of Guizhou Province, China (Figure 1). The transition area between the Yunnan-Guizhou Plateau and Guangxi's hilly plain has a unique karst landscape (Ji et al., 2004; Jiang and Ji, 2013; Cao et al., 2018). The geological environment is fragile and under severe pressure due to both environmental factors and anthropogenic activities. The total area of Dafang is approximately 3505.21 km^2; it belongs to the second step of the Guizhou Plateau and is located in the western part of the

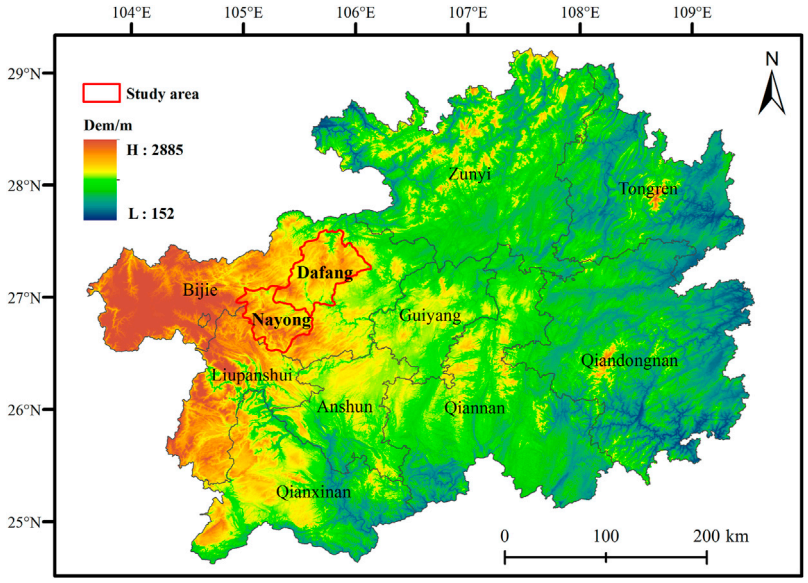

FIGURE 1
Topographic map of Guizhou.

mountain. Dafang has a complex geological structure, and folds and faults are staggered. The karst landforms have various shapes, and the area has dense vegetation, abundant energy and mineral resources, and serious mining operations. In addition, the total area of Nayang is approximately 2452.32 km^2; it belongs to the second step of the Guizhou Plateau and is located in the western part of the Longshan Mountains, east of the northeast line of Longchang, where a series of folded fractures are arranged in the northeast direction. There are ditch and river slopes, Lezhi slopes, and roadside slopes. West of the first line of Longchang is a fold that is parallel to the northeast, which includes the Baogushan anticline, the Yinchanggou anticline, the squat anticline, and the cloak anticline; it is a Chinese-style structure. The mineral resources in the region are rich, and mining is prominent. As a result, many geological disasters such as landslides, collapses, and mudslides have been caused by mineral development in many areas of Bijie.

2.2 Data sources

ALOS-2 is a high-resolution spaceborne synthetic aperture radar that can be used to monitor the movement of Earth's crust and its environment; its band has a wavelength of 150–300 mm, which strongly penetrates vegetation and clouds and is suitable for deformation monitoring in such areas. ALOS-2 can obtain observational data regardless of climatic conditions and time. Therefore, images of a variety of different resolutions, from 1 to 100 m, can be obtained with the help of this radar.

We used long-range ALOS-2 PALSAR stripe model HH-polarization 3-m-resolution descending-track data to characterize six different scenes in the study area. Using the ALOS-2 PALSAR data from 13 September 2016 to 22 November 2016, the potential landslide hazards in the village of Shiping in Yinjiazhai were monitored. In addition, on 30 October 2017, an on-site inspection field visit to the town of Zongling was carried out. Using ALOS-2 PALSAR data from 11 June 2017 and 6 August 2017, the hazards of Zongling disasters were monitored.

2.3 Methodology

2.3.1 Registration

The co-registration stage, with enhanced spectral diversity (ESD), is one of DInSAR's most significant initial steps. Co-registration ensures that a single pair of ALOS-2 PALSAR images are completely aligned so that they can be related pixel-by-pixel to efficiently correct geometric aberrations in the SAR sensors. In order to prevent the geometric phase de-correlation effect, the accuracy of co-registered ALOS-2 PALSAR images should normally be realtively high. As a result, co-registration was performed at the start of DInSAR processing to estimate the ESD correction (range and azimuth offsets) for a subswath. The application of an orbit file, back-geocoding, and ESD are the first steps in the procedure.

To carry out the co-registration of the SAR image pairs, we resampled the DEM reconstructed by DInSAR. The basic principle of DInSAR acquisition *via* DEM technology is to use

two SAR antennas with interference imaging capability (or one SAR antenna with repeated observation) to obtain two coherent univisual complex images with a certain angle difference in the same area; surface elevation information is obtained from their interference phase, so as to reconstruct the ground DEM. DInSAR acquisition of DEM requires a single look complex (SLC) image with good coherence as the data source.

2.3.2 The interference phase

The interferogram contains accurate information on the difference between the slope-up point and the position of the two antennas. The differences include atmospheric delay effects, flat terrain effects, topographic relief, noise, and slight changes in the two imaging processes on the surface. Therefore, when distortion occurs between two acquired images, Eq. 1 is used to remove the flat phase, topographic phase, atmospheric phase, noise, and parameter k from the interference phase to obtain the deformation phase:

$$\varnothing_{int} = \varnothing_{falt} + \varnothing_{top} + \varnothing_{atm} + \varnothing_{mov} + \varnothing_{noise} + \boldsymbol{k} \cdot \boldsymbol{2\pi}, \quad (1)$$

Here, $\varnothing_{\mathrm{int}}$ is the interference phase, $\varnothing_{falt}$ is the flat phase, which can be removed by accurate baseline estimation; $\varnothing_{top}$ is the topography phase, which can be removed by introducing external DEM data; $\varnothing_{mov}$ is the phase changes due to the movement of a target object along the direction of the Line of sight (LoS) during two observations; $\varnothing_{atm}$ is the phase delay caused by atmospheric fluctuations during the transmission of radar electromagnetic waves and can be applied to increase the signal-to-noise ratio between the deformation information and the atmospheric interference signal and to reduce the phase component thereof by using an interferogram superposition method; $\varnothing_{noise}$ is the noise error, and an adaptive filtering method can be used to suppress noise in interferograms; k is ambiguity, and the phase unwrapping method can be used to restore the true phase.

The accuracy and reliability of an interferogram, which are limited by dissimilar phases, will have a significant impact on subsequent DInSAR processes, such as phase unwrapping. In order to achieve the best results, the geometric decorrelation effect in the SAR interferogram should be removed. The geometric decorrelation can be reduced to some extent by filtering the phase differences in a single pair of SLC images appropriately. The interferogram phase filtering is not only suitable but also plays a vital role when we convert the phase into displacement. Among the different phase filtering methods, Goldstein geometric distortions have been used to eliminate the geometric distortion from phases. Goldstein phase filtering has the following steps to improve the estimated accuracy.

1) Choose the adaptive filter of window size 15 × 15 pixels. 2) Calculate fringe frequency in each filtering window. 3) Analyze the fringe frequency and extract the original noisy phase to maintain the fringe appearances.

The noisy phase is then corrected using a modified Goldstein filter. The coherence map and noisy phase frequency already obtained are needed to determine the alpha parameter of the modified Goldstein filter. From this alpha parameter, we can convert the phase error to the required accuracy after combining the previously extracted phase frequency and filter noisy phase to create a final less-geometrically decorrelated interferogram. After filtering, the swath width available in the interferogram, also known as the SAR bursts line should be removed.

2.3.3 Phase unwrapping

The next step in DInSAR data processing is phase unwrapping, which corrects atmospheric, topographic, and geometric distortions in the SAR images by considering the phase differences between neighboring pixels. The task after phase unwrapping is to convert phase to displacement and elevation. In this work, the following mathematical expression is used to find the displacement values from the phase:

$$\Delta \boldsymbol{d} = \left(\varnothing_{unwrap} \times \boldsymbol{\lambda}\right) / -\boldsymbol{4\pi} \times \left(\boldsymbol{cos}\, \boldsymbol{\theta}_{incidence}\right), \quad (2)$$

where, $\Delta \boldsymbol{d}$ = vertical LOS displacement,

$\varnothing_{unwrap}$ = interferogram phase unwrapping,
$\boldsymbol{\lambda}$ = wavelength of SLC C band SAR image, and
$\boldsymbol{\theta}_{incidence}$ = incidence angle.

This expression gives us relative displacement, but we are interested in the absolute mean displacement value. Therefore, for absolute displacement, we subtract the whole image from the coordinated pixel value of the stable point selected in this work and find the mean value of displacement as required. We obtained the before and after LOS displacement and DEM of that region similarly, using phase unwrapping and stable points' coordinated pixel value.

2.4 Flow chart of the two-pass differential interferometric synthetic aperture radar technique

DInSAR, as a general technique, includes methods ranging from single-pair interferometry to more advanced approaches. Higher accuracy can be achieved by using two images obtained over the same location at different times to precisely (Lu et al., 2012) quantify relative distances. We used ALOS-2 PALSAR datasets for DInSAR processing to analyze the study area. The DInSAR processing evaluates the displacement of the ground using the phase difference of the SAR image pairs in the line-of-sight direction. DInSAR processing was carried out to create a phase interferogram for each pair of ALOS-2 PALSAR images of the study area. We obtained the relevant displacement

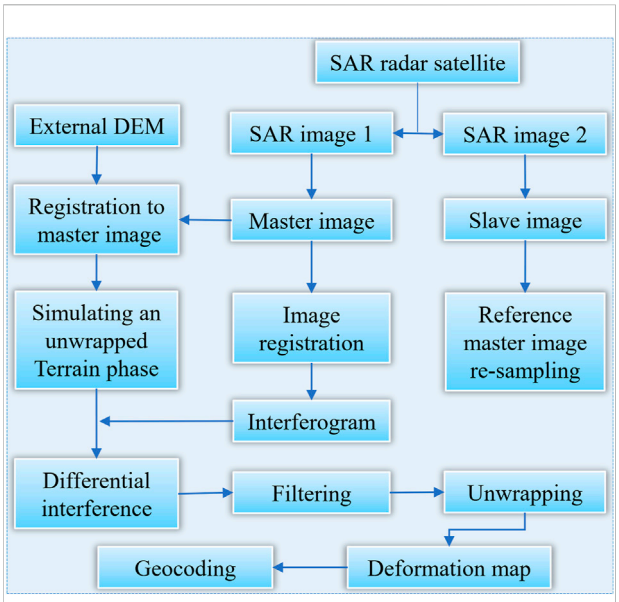

FIGURE 2
Flow chart of the two-pass DInSAR technique.

information and coherence information for processing this phase further. The workflow of DInSAR is shown in Figure 2.

3 Results

3.1 Analysis of undiscovered hazard points in landslide logs

Using the ALOS-2 PALSAR data from 4 September 2016 to 22 January 2017, the local disaster hazards in Yinjiazhai were monitored. The interference between the two scenes constituted a vertical baseline of −167.4 m, and the time baseline was 118 days. Undiscovered hidden points in the landslide account were found in Yinjiazhai of Dafang County, Bijie City. The topography of the area is undulating and mountainous, having many streams and rivers. As typical of karst landscapes, shadows were formed on the radar images. The incidence angle of DInSAR was 36.6° and largely avoided the occurrence of shadows. The landslides in the county mainly occurred in the Quaternary residual strata of bedrock, whereas some occurred in the hard rock and soft rock engineering geological rock group. Collapses occurred mainly in the hard-rock-like strata of carbonate rocks. Figure 3A shows a differential interference fringe map of the Yinjiazhai area, and Figure 3B shows the corresponding geographical position. The lower color scale represents the phase shift corresponding to 11.5 cm [i.e., half the wavelength (23 cm)]. In all the interferograms, several white pixels can be observed, which do not represent real data values. This is due to the geometric distortion, perspective, and shadow effects of the radar signals. In Figure 3C, an enlarged explosive reservoir and coal mining site can be seen on the right and left sides of the mountain, respectively. A landslide body displacement trend is also shown in Figure 3C. There is a large village down in the valley on the right side of the landslide. Thus, landslides could be lethal at this location.

On 30 October 2017, we conducted an on-site investigation field visit of the Yinjiazhai area (Figure 4). The landslide area of this hidden danger is located 500-m east of Yinjiazhai, Dafang County, Bijie City. From on-site inspection photographs and local hydrogeological data, it was revealed that the area has a thick vegetation soil layer. The characteristics of the rock mass are those of Late Permian-Early Triassic siliceous terrigenous clastic and siliceous rocks. The soil is characterized by yellow clay; it has a loose structure, develops shrinkage and cracks, and has poor stability. Small-scale slip has occurred in the soil. The slippage of the landslide was accompanied by yellow mud and some clastic rock. Below the monitored landslide area there is a coal mining area and a large village (Figure 4).

The monitored landslide area is 1200 m wide and has an average slope of 40° with respect to the ground. During the field visit, cracks with a height of 10 cm were observed in the rock, as shown in Figures 4A,B. Rockfall occurred in September 2017. At the time of the visit, the site was undergoing mountain reinforcement and the removal of dangerous rocks. Figure 4B shows the location of (Bardi et al., 2016) the explosives storeroom of the coal mine, which was potentially dangerous. Thus, the people living in the area were relocated to safe areas.

3.2 Hidden points in landslide accounting

Using the ALOS-2 PALSAR data from 13 September 2016 to 22 November 2016, the potential landslide hazards in Shiping were monitored. The interference between the two images constituted a vertical baseline of 50.242 m and a time base of 70 days. The discovered potential hazards in the landslide log book were the mountain hazards in southwest Shiping village, Dafang County, Bijie City.

The monitoring area is located on the transitional slope between the northwest Yunnan Plateau (Yunnan-Guizhou Plateau) and Guizhou Zhongshan Hill. It is a type of Zhongshan landform. The topography of the terrain is undulating and typical of karst topography. Figure 5A shows a differential interference fringe map of the Shiping area, and Figure 5B shows the corresponding geographical position. The calculated deformation of this area is shown in Figure 5C. The geographical coordinates of the monitored landslide area are 27°15′48.74″N, 105°44′35.47″E, and the deformation is 7.8 cm.

On 30 October 2017, an on-site inspection field visit of the area was carried out. The situation of hidden danger points was

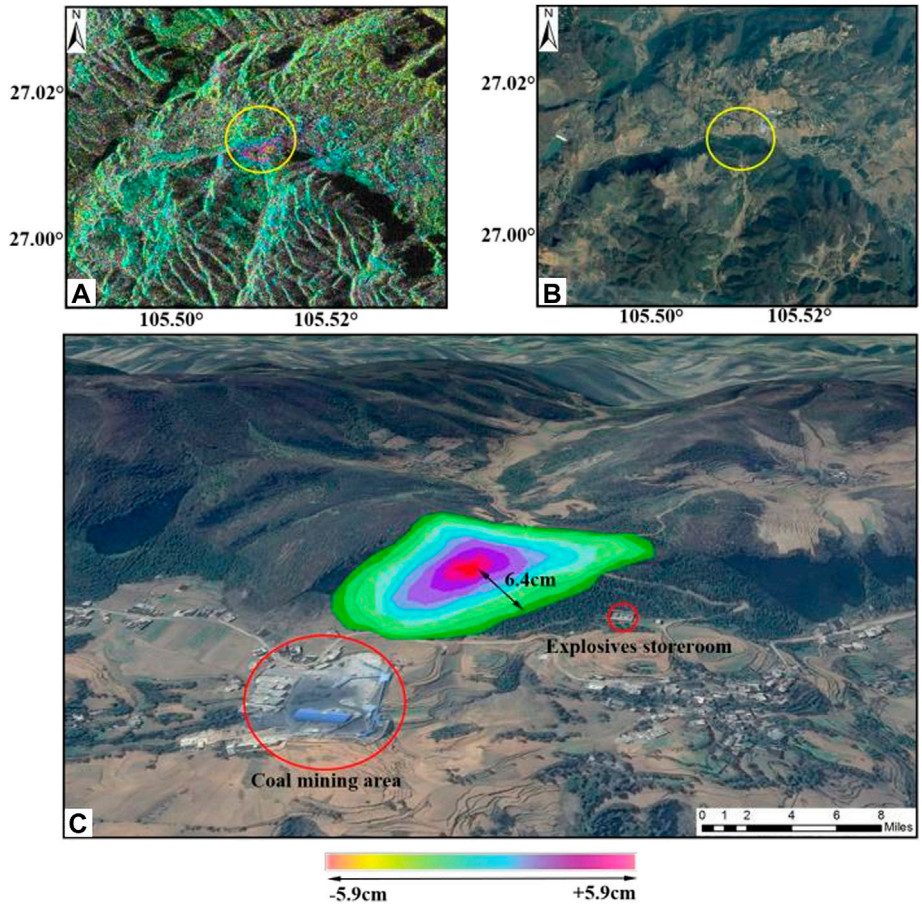

FIGURE 3
The DInSAR Yinjiazhai village results.

specifically shown in Figure 6. A hidden landslide area is located in the vicinity of the mountain to the southwest of Shiping, adjacent to the coal mining site. According to the site investigation photographs shown in Figures 6A–C, there have been ground fissures in some areas of the mountain. Figure 6C and local hydrogeological data reveal that the characteristics of the mountain body are those of Late Permian-Early Triassic early siliceous terrigenous clastites and siliceous rocks, which show massive structures and soft rocks. The body of the mountain is mainly composed of yellow clay with a block structure. The yellow clay has high water saturation and shrinkage. Seasonal rains and human activities, combined with the nature of yellow clay, can increase the chance of landslides. The DInSAR monitoring results from September to November 2016 showed that large deformations have occurred in the landslide area. During the field visit, large cracks on the surface were found. The length of surface cracks in the southwest direction of Shiping Village was 2.8 m. On 13 July 2017, Shiping collapsed as a result of the collapse of the mountainous area where the disaster occurred. Roads and pig farms were badly damaged during the incident. Figure 6C shows that the landslide was a bedrock landslide. In addition, from Figure 6C, we can clearly distinguish the three elements of the landslide: the back wall, the body, and the sidewall. The average slope of the landslide in the landslide area was approximately 65°. The landslide height was 95 m, while the length and width were 150 m and 25 m, respectively. The landslide was 5-m thick. The sliding body material was composed of broken bedrocks that were covered with a thin layer of loess. The composition material was dominated by crushed stone. The scale of the landslide was mainly small, and the landslide was primarily thin. Its accumulation form was generally complete, showing a clear circular chair shape, with a steep back wall and a slope of approximately 60–70°. From the mechanics analysis, it was a towed landslide. At the time of the visit, the front edge of the landslide was loosely broken, and there were obvious signs of continued deformation. Sliding is expected during rainfall in the area.

FIGURE 4
Field check photos of Yinjiazhai.

3.3 An analysis of hidden points

Using the ALOS-2 PALSAR data from June 11 to 6 August 2017, local disasters in the study area were monitored. The interference between two images constituted a vertical baseline of 212.61 m, and the time baseline was 56 days. It was discovered that a hidden point of landslides occurred on the 420 m northwest mountain near Zongling. Figure 7 shows that the landslide area is widely distributed, there are multiple landslide bodies, and there is a village below the landslide.

The rocks of the study area formed a soft and hard interbedded layer, and a weak structural plane was formed on the contact surface, making the rock and soil easy to slide. The weak structural surfaces were slippery and misaligned, which (Raetzo et al., 2007) favored the production of hidden hazards such as landslides and collapses. A landslide was detected in the town of Zongling in Nayong County. Due to the abundance of mineral resources in the area, artificial mining has caused many geological hazards. In the differential interference fringe diagrams of Figures 8A,B, the topographic phase cannot be completely removed due to the insufficient accuracy of the external DEM used. Figure 8A shows the results of the observations from 2016, and Figure 8B shows those from 2017. Comparing the two figures, it can be determined that the hidden landslide points slipped for two consecutive years, with an average slip of 6.0 cm. Figures 8C,D show the actual locations of this hidden hazard in 2016 and 2017, and Figures 8E,B show the calculated deformation of this area. The geographic coordinates of the landslide area are 26°42′49.17″N, 105°14′29.02″E.

We observed that the above-mentioned hidden danger point was in the local landslide account books (Marko et al., 2015). We conducted an on-site verification field visit on 31 October 2017. The area receives high amounts of rainfall during May and June. The large amount of precipitation has led to an increase in the groundwater table in the area. The chance of landslides increases with rainfall amount. The disaster in this area is located in the large Mazongling coal-mining area. There are numerous nearby coal mines, with a total of more than 20 coal-mining companies, and the extent of mining is very large. These mines greatly impact landslides and disasters in the region. The monitoring results from 2015 showed that only the major landslides were deformed, and only significant deformations were found at the two landslide points. According to the monitoring results from 2017 and the inspection photographs shown in Figures 9A,B, there are many large-scale deformations in Mazongling as a whole, and there are many villages in the valley. The landslide belt was 4.29 km long along the direction of the mountain. In addition, from Figure 9B, we can clearly distinguish the three elements of the landslide: the back wall, the body, and the sidewall. The characteristics of the mountain rock mass are those of Late Paleozoic and Triassic carbonate rocks and Early Permian to Early Triassic siliceous terrestrial clastic and siliceous rocks. There is a bulk structure and soft-rock fragment structure, the soil is yellow clay, and the northern soil is thick and has a loose structure. From the mechanics analysis, these areas are traction landslides. At the time of the field visit, the front

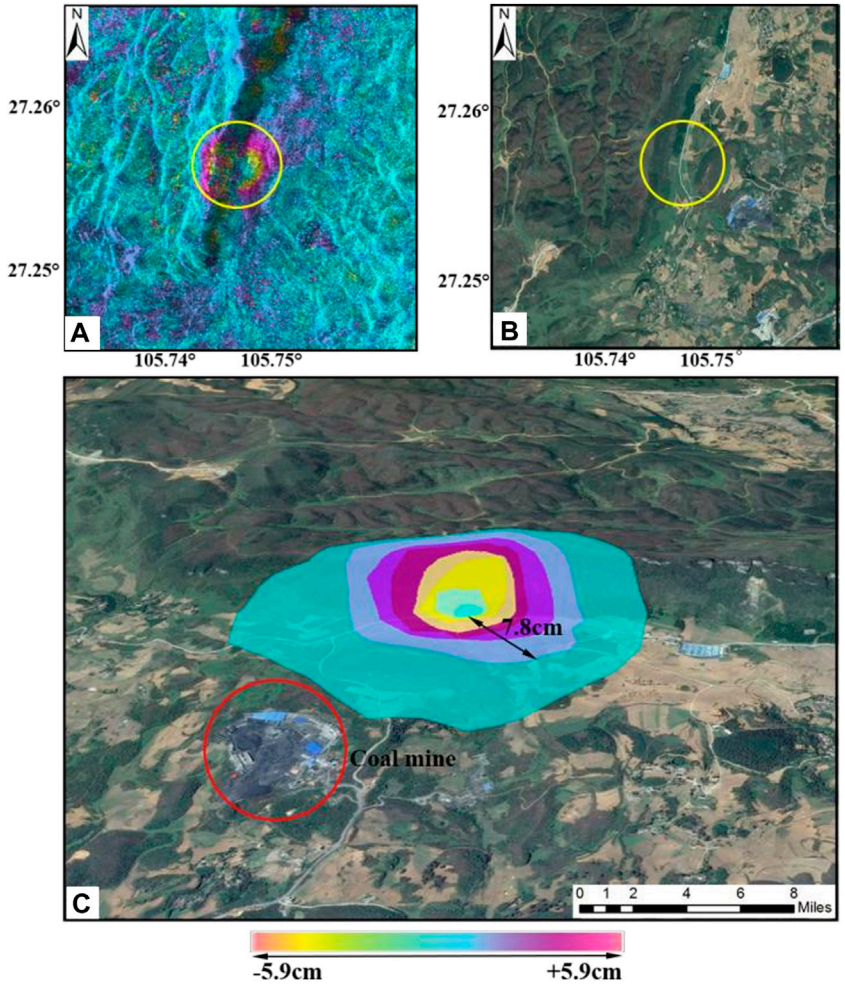

FIGURE 5
The DInSAR results of Shiping village.

edge of the landslide was loosely broken, and there were obvious signs of continued deformation. The town of Zongling lies below the southern foothills of the mountain. There are 1402 households in the town, with a population of 9220 individuals.

4 Discussion

Landslides are one of the most destructive geological disasters, and they are characterized by high speed, long runout distance, and great impact on terrain (Xu et al., 2015; Zhang et al., 2016; Chen et al., 2018; Ali et al., 2020). Geological structure, stratum lithology, topography, meteorology, and human activities often trigger catastrophic landslide events. Bijie is among the areas highly prone to landslides. Therefore, it is necessary to carry out research on the factors impacting landslide geology disaster (Frodella et al., 2016) susceptibility evaluation in the study area (Gang, 2016).

4.1 Geological structure and formation lithology

The geological structure within Bijie City is relatively complex (Figure 10). Folding faults are well-staggered and contain two tectonic units: the Qixingguan northeast structural deformation zone and the northeast-facing folded fault (Gong and Zhao, 2009). The development and outcropping of the sedimentary strata in the country are relatively complete, ranging from the Sinian in the Proterozoic to the Quaternary in the Cenozoic, except for the Baidai Formation. The exposed rocks in the territory are mainly (Herrera et al., 2011) sedimentary rocks, the area of

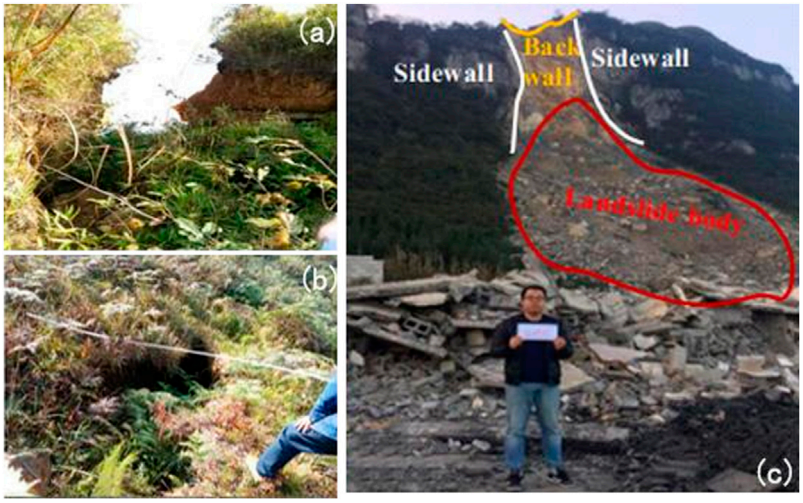

FIGURE 6
Field visit photographs of Shiping village.

FIGURE 7
Panoramic view of Zongling and nearby mountains.

which is approximately 24,900 km^2, accounting for 92.8% of the total area of the city; magmatic rocks are less widely distributed, with an exposed (Carla et al., 2016) area of approximately 0.19 million km^2 that accounts for 7.2% of the total area. Among the sedimentary rocks, there are mostly carbonate rocks with an exposed area of approximately (Lu et al., 2014) 16,700 km^2, accounting for 62.2% of the total area. The exposed area of coal-base sand shales is approximately 0.49 million km^2, accounting for 15.6% of the total area (Cigna et al., 2013). Regarding purple sand, the exposed area of shale and mauve sand mudstone is approximately 0.37 million km^2, accounting for 12.9% of the total area. The exposed area of muddy rocks is 0.05 million km^2, which accounts for 2.1% of the total area.

Dafang County is located in the northwest of the Jurassic Fold Belt in Guizhou Province (Intrieri et al., 2018); its structural outline consists of a series of north-northeast tight folds and near east-west faults, near north-south faults, or fault bundles. The main faults are the Laojing-Daxi fault zone, the Yangchangba-Machang fault zone, the Dingxin fault belt, and the Dashan fault zone. The tectonic units of the monitoring area are the NE-trending tectonic deformation area of the Zunyi fault in the (Toshitaka, 1998) Yangtze quasi-platform and the NE-trending tectonic deformation area of the Bijie in the northern Guizhou platform. The fault structure in Nayong County, located in the southwest section of the northwest wing of the Zhijin Santang syncline, is relatively developed. Exposed limestone structural planes are developed, and there are multiple groups of steeply dipping structural planes. The limestone is cut into massive and sub-massive units.

Nayong County is located in the NE-trending Bijie structural deformation area of the Zunyi fault arch in the northern Guizhou platform of the Yangtze quasi-platform. Folds and faults are well developed, and the bearing of the structural line changes greatly. Fractures are developed, the rock mass is broken, and its integrity is poor.

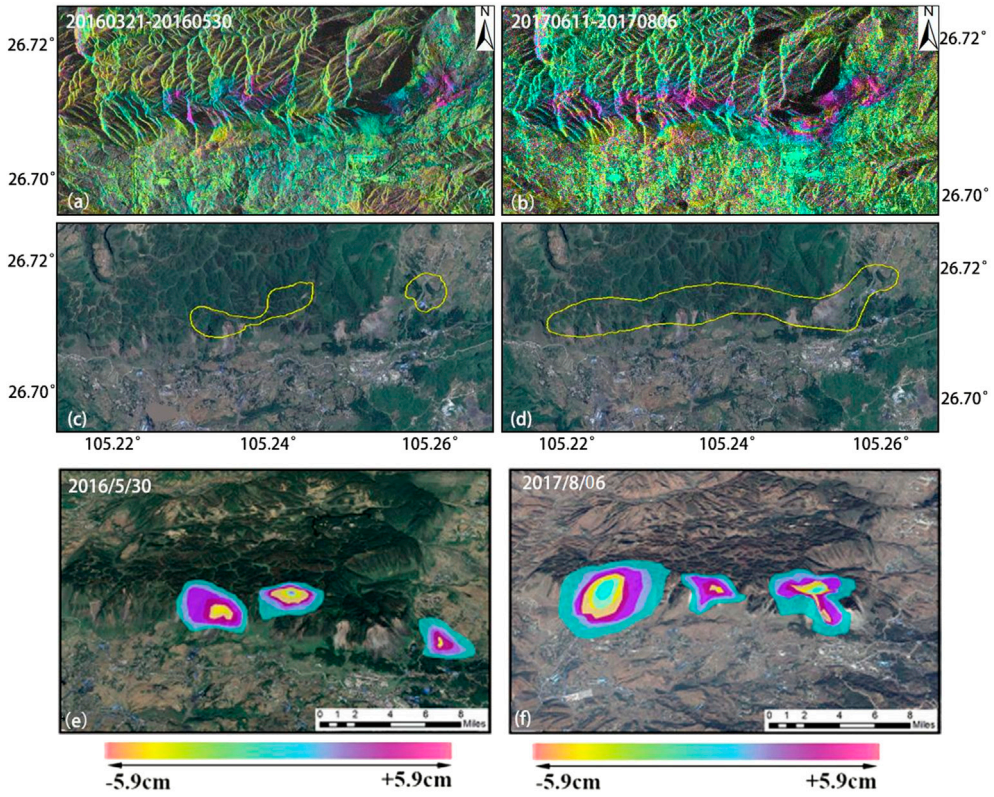

FIGURE 8
The DInSAR results of Zongling.

FIGURE 9
Field visit photographs of the landslide in the town of Zongling.

In addition, as a manifestation of neotectonic movement, earthquakes directly impact landslide disasters. According to Wang et al. seismological zoning (Wang et al., 2017), most of the Bijie area is located in the seismic belt of the middle reaches of the Yangtze River, and a few areas are located in the Youjiang earthquake zone. The seismic activity in these seismic zones is relatively weak, which is mainly dominated by medium and strong earthquakes of magnitude 5 with low frequency. However, the high susceptibility of earthquakes directly leads to an unstable regional geological structure and landslide hazards. According to historical records and site investigations, some of the old landslides in the area were directly caused by earthquakes.

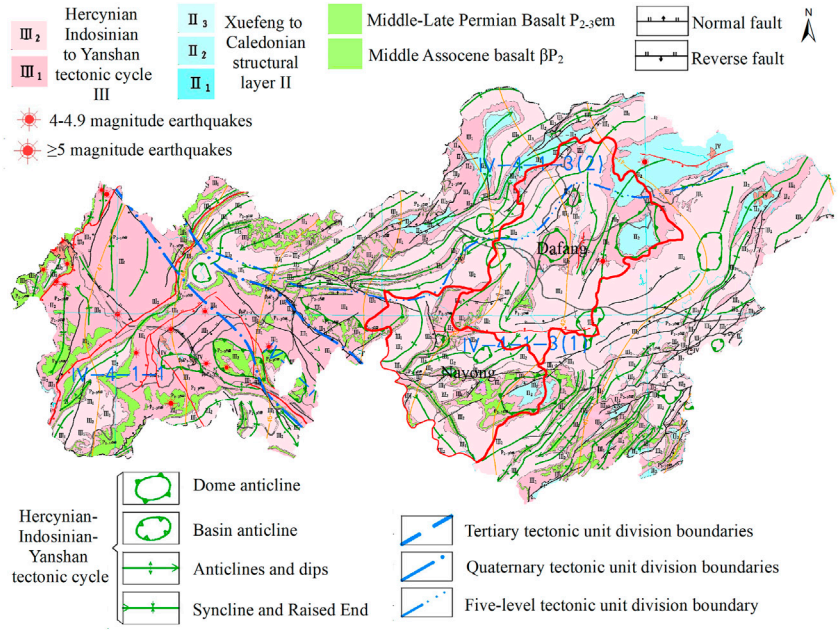

FIGURE 10
Geological structure map of Bijie.

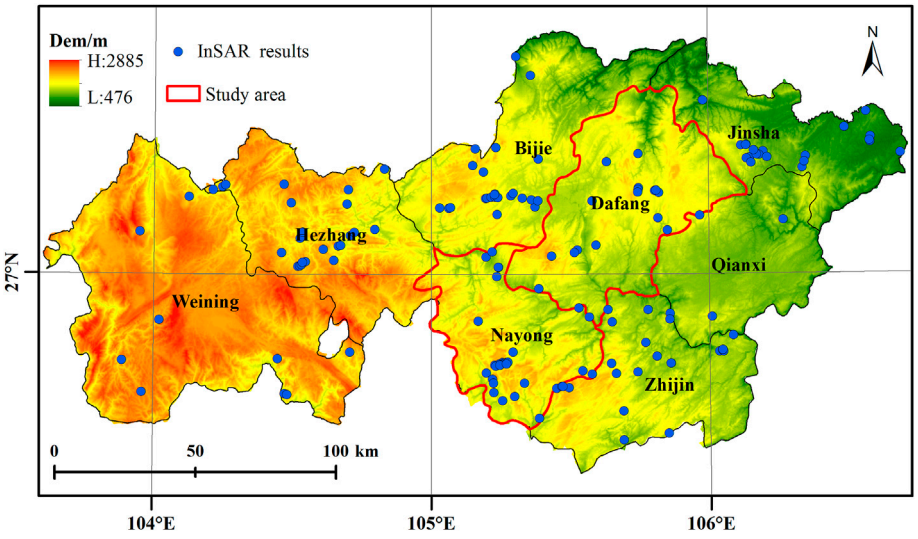

FIGURE 11
DInSAR potential landslide distribution.

4.2 Topography

Bijie City is located at the slope of the transition from the Yunnan Plateau to the central hills of Guizhou Province. The terrain is undulating and strongly cutting. The overall terrain is high in the west and low in the east and has a ladder-like distribution. The territory is mountainous, with the main mountain ranges being Wengeng Mountain in the west and north Dagu Mountain and Laowang Mountain in the southwest. Wumeng Mountain is located in the western parts of Hezhang

County and Weining County, and it is the watershed of the Niulan, Baishui, Beipan, and Wu rivers. Its mountain range is the watershed of the Wu and Yangtze rivers in Bijie City. The Laowang Mountain range extends northwest and southeast, and the northwestern end connects with the eastern Wumeng Mountain and extends eastwards. Liushui City's Shuicheng and Liuzhi areas are divided into the watersheds of the Sancha River upstream of the Wu River and the Beipan River of the Pearl River system. The landform of the study area belongs to the plateau mountain in the southwestern part of China, which is located in the eastern part of the Yunnan-Guizhou Plateau. The terrain is high in the west and low in the east, tilting from the center to the north, east, and south, with an average elevation of 1100 m. Located in the central belt of the karst region in southwest China, its unique topography and geomorphology also create terrain conditions favorable for landslide formation.

The landslide area of Dafang County is located in the western part of the Yunnan-Guizhou Plateau (Figure 11). The landform types are mainly eroded and dissolved low-mountain landforms. The highest elevation is 1640 m, and the lowest is 1440 m. The maximum relative height difference is approximately 200 m. The terrain slope in the area ranges from 30° to 50°, with local steep cliffs reaching over 80°. In addition, the landform in the area where the landslide is located in Nayong County is a low-medium mountain landform of tectonic erosion and denudation, and the overall topography is high in the south and low in the north. The topography of the collapse area is steep on the top and gentle on the bottom. The source area of the collapse is a steep mountain with a slope greater than 70° formed by the Triassic Feixianguan Formation, with a maximum elevation of 2175 m. The collapse body movement area is mainly composed of the Permian Longtan Formation coal-measure strata. The overall terrain is gentle, with a maximum slope of 5° and a minimum elevation of 1875 m.

4.3 Meteorological and hydrology

Studies have shown that the interaction of rainfall with topography, soil lithology, vegetation, and population density is closer to the spatial distribution of fatal landslides than each individual factor (Lin and Wang, 2018; Liu and Miao, 2018). In addition, an increase in extreme weather is also one of the factors of landslide occurrence (Ali et al., 2020; Ali et al., 2021). Bijie has a humid subtropical monsoon climate, rainfall is relatively abundant, and the three-dimensional climate is outstanding. There are many types of disastrous weather, and extreme weather events such as drought and flood, as well as cold and heat, occur frequently.

The average annual rainfall in Dafang County is 1180 mm. The average temperature is 11°C, with a maximum of 31°C and a minimum of −9°C. The frost-free period is approximately 265 days, and the dominant wind direction is to the southeast. The county belongs to a subtropical humid monsoon climate. Due to the sudden change of terrain, the climate changes greatly, and the temperature difference between mountains and valleys is large. Dafang County belongs to the Yangtze River Basin, which belongs to the Wujiang River and Chishui River system.

The rainfall in Nayong County is mainly concentrated from May to August, accounting for more than 70% of that for the whole year, and the annual average rainfall is 1243.9 mm. In a year, June has the most rainfall, with an average rainfall of 223.0 mm, and December has the least, with an average of 22.0 mm. The distribution of precipitation increases from northwest to southeast, where the southeast is a rainy area with a total annual precipitation of more than 1300 mm, whereas the annual total rainfall in the northwest is less than 1000 mm. Heavy rain is generally concentrated in May–September (; Zhai, 2019). According to meteorological data, the maximum temperature is expected to be 32.4°C, and the minimum is −7.2°C.

4.4 Human activities

From 2016 to 2017, the rainfall was very low, but the deformation rate of Zongling was as high as 0.6 mm per day, which indicates that there are factors other than rainfall affecting the surface deformation. It was found that the geological and lithological properties of this area were weak, with a large number of coal-bearing strata. Coal mining activities led to the occurrence of ground subsidence and ground cracks. The rich mineral and coal resources in the study area intensify such development and utilization. Landslides, collapses, debris flows, and other geological disasters often occur in Zongling due to this mineral development. These geological disasters have seriously threatened the safety of life and property in the surrounding towns and villages of mining enterprises for many years.

4.5 Advantages and disadvantages of differential interferometric synthetic aperture radar

DInSAR technology is a measurement technology that uses two complex SAR images in the same area at different time phases for interference processing and obtains elevation and surface deformation information according to phase information (Bamler and Hartl, 1998; Tomas et al., 2014). DInSAR technology has the advantages of high deformation, high resolution and is not affected by weather. It can make up for the shortage of traditional total station, global positioning system and precision leveling instrument, and reveal the surface information of the measured domain more deeply. In addition, DInSAR technology can quickly monitor landslide

displacement in a larger spatial range due to its advantages of revisit cycle, remote monitoring, and low cost. It can greatly improve the efficiency, accuracy and reliability of monitoring geological hidden danger points in complex terrain areas (Cascini et al., 2009; Zhao et al., 2012). DInSAR technology is a good supplement to traditional landslide disaster monitoring methods, showing great potential in landslide disaster investigation in large areas (Colesanti and Wasowski, 2006).

Traditional DInSAR technology focuses on the study of single deformation, which uses few SAR images, but has very high requirements on SAR images. Firstly, the single deformation should ensure that the baseline distance is relatively small, and the time interval of SAR data should not be too large, otherwise the interferogram will be affected by geometric and temporal decoherence. Secondly, the single deformation requires very high accuracy of DEM, and the atmospheric influence is difficult to eliminate. Therefore, there are two—and three-track DInSAR techniques in common use today. The advantage of the two-track method is that it does not need to phase untangle the interferogram to avoid the difficulty of understanding the entanglement. The disadvantage is that accurate registration of DEM and SAR images is required. The advantage of the three-track method is that it does not need to consider the registration problem, but it needs to untangle the interferogram phase.

5 Conclusion

Through the analysis of differential interferograms, the potential hazards of disasters in the study area were rapidly identified. Based on the results and on-site verification analyses, the following conclusions can be drawn.

(1) The DInSAR results showed that undiscovered hidden points in the landslide account were found in Yinjiazhai. In addition, the deformation of the differential interference fringe map was 6.4 cm. It was observed that the landslide slipped with yellow mud and some clastic rocks, and there were 10-cm-wide cracks in the rocks. The average slope of the landslide in of Shiping area was approximately 65°. The landslide height was 95 m, the length and width were 150 m and 25 m, respectively, the thickness was 5 m, the deformation was 7.8 cm, and the length of surface cracks was 2.8 m. The entire Zongling landslide was a traction landslide, with large-scale deformation in many places, and the landslide zone in the direction of the mountain was 4.29 km long. In addition, three elements of the landslide can be clearly seen in the study area: the rear wall, the body, and the sidewall.

(2) Through three examples, the landslides detected after the rainy season in the four research areas and some of the observed deformations in the mining areas have been very useful to assess the damage that could be potentially caused by these slow movements. They provide new technical means for monitoring potential hazards in the landslide-prone areas of southwest China. For areas covered with dense vegetation in mountainous areas, DInSAR can quickly and accurately find abnormal points, effectively judge the development trend of outliers, and provide early warning of potential danger.

Data availability statement

The original contributions presented in the study are included in the article/supplementary material, further inquiries can be directed to the corresponding author.

Author contributions

All authors contributed to the study conception and design. Material preparation, data collection and analysis were performed by CS, SZ, XL, YZ, and HL. The first draft of the manuscript was written by CS and all authors commented on previous versions of the manuscript. All authors read and approved the final manuscript.

Funding

This research work was supported jointly by the Outstanding Youth of Science and Technology program of Guizhou Province of China [(2021)5615], the Department of Science and Technology program of Guizhou Province of China ([2022] 213 and [2023]60).

Acknowledgments

We thank the editor and reviewers for giving us many opportunities to revise for helping us improve the quality of the paper.

Conflict of interest

The authors declare that the research was conducted in the absence of any commercial or financial relationships that could be construed as a potential conflict of interest.

Publisher's note

References

Agostini, G., Casagli, N., Delmonaco, G., Fanti, R., and Margottini, C. (2002). Landslide monitoring and cultural heritage at risk: The case study of san miniato hill in florence. *EGS General Assem. Conf. Abstr.* 45, 455.

Ali, R., Kuriqi, A., and Kisi, O. (2020). Human environment natural disasters interconnection in China: A review. *Climate* 8 (4), 48. doi:10.3390/cli8040048

Ali, R., Shu, H., Kuriqi, A., Siddiqui, S. S., Gagnon, A., Lu, L. L., et al. (2021). Characterization of the 2014 indus river flood using hydraulic simulations and satellite images. *Remote Sens. (Basel).* 13 (11), 2053. doi:10.3390/rs13112053

Alice, T. H., Agnès, H., Jean-Philippe, M., Jean, S., Alessandro, C., and Manfred, J. (2013). Seismic monitoring of soft-rock landslides: The super-sauze and valoria case studies. *Geophys. J. Int.* 193 (3), 1515–1536. doi:10.1093/gji/ggt039

Ayalew, L., Yamagishi, H., Marui, H., and Kanno, T. (2005). Landslides in sado island of Japan: Part I. Case studies, monitoring techniques and environmental considerations. *Eng. Geol.* 81 (4), 419–431. doi:10.1016/j.enggeo.2005.08.005

Bamler, R., and Hartl, P. (1998). Synthetic aperture radar interferometry. *Inverse probl.* 14 (4), R1–R54. doi:10.1088/0266-5611/14/4/001

Bardi, F., Raspini, F., Ciampalini, A., Kristensen, L., Rouyet, L., Lauknes, T., et al. (2016). Space-Borne and ground-based InSAR data integration: The åknes test site. *Remote Sens. (Basel).* 8 (3), 237. doi:10.3390/rs8030237

Cao, X., Wu, P., Zhou, S., Zhou, S., Han, Z., Tu, H., et al. (2018). Seasonal variability of oxygen and hydrogen isotopes in a wetland system of the yunnan-Guizhou Plateau, southwest China: A quantitative assessment of groundwater inflow fluxes. *Hydrogeol. J.* 26 (1), 215–231. doi:10.1007/s10040-017-1635-8

Carlà, T., Raspini, F., Intrieri, E., and Casagli, N. (2016). A simple method to help determine landslide susceptibility from spaceborne InSAR data: The montescaglioso case study. *Environ. Earth Sci.* 75, 1492. doi:10.1007/s12665-016-6308-8

Cascini, L., Fornaro, G., and Peduto, D. (2009). Analysis at medium scale of low-resolution DInSAR data in slow-moving landslide-affected areas. *ISPRS J. Photogrammetry Remote Sens.* 64 (6), 598–611. doi:10.1016/j.isprsjprs.2009.05.003

Catani, F., Farina, P., Moretti, S., Nico, G., and Strozzi, T. (2005). On the application of SAR interferometry to geomorphological studies: Estimation of landform attributes and mass movements. *Geomorphology* 66, 119–131. doi:10.1016/j.geomorph.2004.08.012

Cigna, F., Bianchini, S., and Casagli, N. (2013). How to assess landslide activity and intensity with persistent scatterer interferometry (PSI): The PSI-based matrix approach. *Landslides* 10, 267–283. doi:10.1007/s10346-012-0335-7

Colesanti, C., and Wasowski, J. (2006). Investigating landslides with space-borne synthetic aperture radar (SAR) interferometry. *Eng. Geol.* 88 (3), 173–199. doi:10.1016/j.enggeo.2006.09.013

Corsini, A., Farina, P., Antonello, G., Barbier, M., Casagli, N., Coren, F., et al. (2006). Space-borne and ground-based SAR interferometry as tools for landslide hazard management in civil protection. *Int. J. Remote Sens.* 27, 2351–2369. doi:10.1080/01431160600554405

Frodella, W., Ciampalini, A., Gigli, G., Lombardi, L., Raspini, F., Nocentini, M., et al. (2016). Synergic use of satellite and ground based remote sensing methods for monitoring the San Leo rock cliff (Northern Italy). *Geomorphology* 264, 80–94. doi:10.1016/j.geomorph.2016.04.008

Froude, M. J., and Petley, D. N. (2018). Global fatal landslide occurrence from 2004 to 2016. *Nat. Hazards Earth Syst. Sci.* 18, 2161–2181. doi:10.5194/nhess-18-2161-2018

Gang, L. (2016). Analyses of important geo-disasters distribution rules and influence factors of Guizhou. *Guizhou Geol.* 33 (02), 108–112.

Gong, X., and Zhao, X. (2009). Type, causation and prevention of geologic disaster hidden danger in Nayong county. *Guizhou Geol.* 26 (03), 235–237.

Herrera, G., Notti, D., García-Davalillo, J. C., Mora, O., Cooksley, G., Sánchez, M., et al. (2011). Analysis with C- and X-band satellite SAR data of the Portalet landslide area. *Landslides* 8, 195–206. doi:10.1007/s10346-010-0239-3

Hu, X., Wang, T., Pierson, T. C., Lu, Z., Kim, J., and Cecere, T. H. (2016). Detecting seasonal landslide movement within the Cascade landslide complex (Washington) using time-series SAR imagery. *Remote Sens. Environ.* 187, 49–61. doi:10.1016/j.rse.2016.10.006

Intrieri, E., Raspini, F., Fumagalli, A., Lu, P., Del Conte, S., Farina, P., et al. (2018). The maoxian landslide as seen from space: Detecting precursors of failure with sentinel-1 data. *Landslides* 15, 123–133. doi:10.1007/s10346-017-0915-7

Iverson, R. M. (2000). Landslide triggering by rain infiltration. *Water Resour. Res.* 36, 1897–1910. doi:10.1029/2000WR900090

Ji, H., Wang, S., Ouyang, Z., Zang, S., Sun, C., Liu, X., et al. (2004). Geochemistry of red residua underlying dolomites in karst terrains of yunnan-Guizhou Plateau: I. The formation of the pingba profile. *Chem. Geol.* 203 (1-2), 1–27. doi:10.1016/j.chemgeo.2003.08.012

Ji, S., Yu, D., Shen, C., Liu, W., and Xu, Q. (2020). Landslide detection from an open satellite imagery and digital elevation model dataset using attention boosted convolutional neural networks. *Landslides* 17 (6), 1337–1352. doi:10.1007/s10346-020-01353-2

Jiang, Y., and Ji, H. (2013). Isotopic indicators of source and fate of particulate organic carbon in a karstic watershed on the Yunnan-Guizhou Plateau. *Appl. Geochem.* 36 (76), 153–167. doi:10.1016/j.apgeochem.2013.06.005

Lei, G., Yin, K., and Glade, T. (2013). Power-law statistics of a landslide inventory of wanzhou district, three-gorges reservoir, China. *EGU General Assem. Conf. Abstr.* 4, 07–12.

Lin, Q., and Wang, Y. (2018). Spatial and temporal analysis of a fatal landslide inventory in China from 1950 to 2016. *Landslides* 15 (12), 2357–2372. doi:10.1007/s10346-018-1037-6

Liu, X., and Miao, C. (2018). Large-scale assessment of landslide hazard, vulnerability and risk in China. *Geomat. Nat. Hazards Risk* 9 (1), 1037–1052. doi:10.1080/19475705.2018.1502690

Lu, P., Casagli, N., Catani, F., and Tofani, V. (2012). Persistent Scatterers Interferometry Hotspot and Cluster Analysis (PSI-HCA) for detection of extremely slow-moving landslides. *Int. J. Remote Sens.* 33 (2), 466–489. doi:10.1080/01431161.2010.536185

Lu, P., Catani, F., Tofani, V., and Casagli, N. (2014). Quantitative hazard and risk assessment for slow-moving landslides from Persistent Scatterer Interferometry. *Landslides* 11, 685–696. doi:10.1007/s10346-013-0432-2

Malamud, B. D., Turcotte, D. L., Guzzetti, F., and Reichenbach, P. (2004). Landslides, earthquakes, and erosion. *Earth Planet. Sci. Lett.* 229, 45–59. doi:10.1016/j.epsl.2004.10.018

Marko, K., Holley, R., Mahapatra, P., Marel, H. V. D., and Bavec, M. (2015). Coupling of GPS/GNSS and radar interferometric data for a 3D surface displacement monitoring of landslides. *Landslides* 12, 241–257. doi:10.1007/s10346-014-0482-0

Moretti, S., Cigna, F., Raspini, F., Cooksley, G., Banwell, M. J., Raetzo, H., et al. (2013). Use of persistent scatterer InSAR within Terrafirma landslide services. *Landslide Sci. Pract.* 2, 317–323. doi:10.1007/978-3-642-31445-2_41

Othman, Z., Aziz, W., and Anuar, A. (2012). Landslide monitoring at hillside residential area using GPS static and inclinometer techniques. *Proc. SPIE - Int. Soc. Opt. Eng.* 8334, 31. doi:10.1117/12.946079

Raetzo, H., Wegmüller, U., Strozzi, T., Marks, F., and Farina, P. (2007). Monitoring of lumnez landslide with ERS and envisat. *Sar. data* 45, 1333.

Shen, C., Feng, Z., Xie, C., Fang, H., Zhao, B., Ou, W., et al. (2019). Refinement of landslide susceptibility map using persistent scatterer interferometry in areas of intense mining activities in the karst region of southwest China. *Remote Sens. (Basel).* 11 (23), 2821. doi:10.3390/rs11232821

Singhroy, V. (2009). *InSAR monitoring of landslides using RADARSAT//EEE international geoscience & remote sensing symposium*. Cape Town, South Africa: University of Cape TownIEEE. IGARSS 2009, July 12-17, 2009. doi:10.1109/IGARSS.2009.5416925

Tai, Y. H., and Chang, C. P. (2015). Application of radar interferometry for monitoring the landslide creeping of jiufen area, northern taiwan//egu general assembly conference. *EGU General Assem. Conf. Abstr.* 24, 577.

Tofani, V., Raspini, F., Catani, F., and Casagli, N. (2013). Persistent scatterer interferometry (PSI) technique for landslide characterization and monitoring. *Remote Sens. (Basel).* 5 (3), 1045–1065. doi:10.3390/rs5031045

Tomás, R., Romero, R., Mulas, J., Marturia, J. J., Mallorqui, J. J., Lopez-Sanchez, J. M., et al. (2014). Radar interferometry techniques for the study of ground subsidence phenomena: A review of practical issues through cases in Spain. *Environ. Earth Sci.* 71, 163–181. doi:10.1007/s12665-013-2422-z

Toshitaka, K. (1998). Monitoring the process of ground failure in repeated landslides and associated stability assessments. *Eng. Geol.* 50 (1-2), 71–84. doi:10.1016/S0013-7952(97)00085-9

Wang, S., Liang, C., Xing, X. J., Luo, Y., Hao, J., Liu, Y., et al. (2017). Seismic distribution, division and zonation of Guizhou province. *Guizhou Geol.* 34 (01), 1–8.

Wiatr, T., Reicherter, K., Fernándezsteeger, T., and Rodrigues, D. (2009). Mass movement monitoring by terrestrial laser scanning on madeira island (Portugal). *EGU General Assem. Conf. Abstr.* 466, 19.

Xu, C., Xu, X., and Shyu, J. B. H. (2015). Database and spatial distribution of landslides triggered by the Lushan, China Mw 6.6 earthquake of 20 April 2013. *Geomorphology* 248, 77–92. doi:10.1016/j.geomorph.2015.07.002

Yin, Y., Wang, H., Gao, Y., and Li, X. (2010). Real-time monitoring and early warning of landslides at relocated wushan town, the three Gorges reservoir, China. *Landslides* 7 (3), 339–349. doi:10.1007/s10346-010-0220-1

Zainon, O. (2011). Landslide monitoring using global positioning system and inclinometer techniques. *Glob. Position. Syst. Landslide Hazard Anal.* 76, 190.

Zhang, S., Xu, Q., and Hu, Z. (2016). Effects of rainwater softening on red mudstone of deep-seated landslide, Southwest China. *Eng. Geol.* 204, 1–13. doi:10.1016/j.enggeo.2016.01.013

Zhao, C., Lu, Z., Zhang, Q., and Fuented, J. L. (2012). Large-area landslide detection and monitoring with ALOS/PALSAR imagery data over Northern California and Southern Oregon, USA. *Remote Sens. Environ.* 124, 348–359. doi:10.1016/j.rse.2012.05.025

Zou, F., Zhou, Z., and Xu, Y. (2017). Review about geological environment problems of the mines in Guizhou Province. *Environ. Prot. Technol.* 23 (1), 61–64.